Parameter Identification of Bearing Supports From Imbalance Response and Impact Excitations

by

Oscar C. De Santiago

Dr. Luis San Andrés

May 2001

TRC-RD-1-01

PARAMETER IDENTIFICATION OF BEARING SUPPORTS FROM IMBALANCE RESPONSE AND IMPACT EXCITATIONS - PROGRESS REPORT

EXECUTIVE SUMMARY

Identification of on-site bearing parameters proves useful for turbomachinery diagnostics and validation of predictions of rotor dynamic response. This report details the progress on the parameter identification of the integral squeeze film damper-tilting pad bearing series support of the NSF-SFD test rigid rotor. Two suitable methodologies are presented here, namely identification from rotor imbalance response and from impact response measurements. Rotor imbalance response allows identification of synchronous force coefficients, while the impact response allows for identification of frequency-dependent bearing parameters.

At least two linearly independent responses at four locations (two bearing locations, two orthogonal directions) are necessary for reliable identification of bearing coefficients from imbalance response measurements. Parameter identification from impact excitation requires at least two impacts on the rotor at the same running speed. Impacts may be exerted in the same direction at two different axial locations or at the same location but in two orthogonal directions. Least squares error minimization is readily applicable for both methods when redundant data is available.

Numerical simulations show that identification from imbalance responses is adequate for rotor speeds above 60% of the first rigid rotor critical speed with the best identification range located between critical speeds. Satisfactory identification of cross-coupled stiffness requires that the relative magnitude of these coefficients with respect to the main stiffness coefficients is larger than 2%.

Preliminary test measurements for identification of bearing parameters from imbalance responses are not yet satisfactory mainly due to the motion of the flexible pedestals. It is thus necessary to include additional degrees of freedom into the identification procedure to account for the pedestal motions. On the other hand, experimental vibration signatures from preliminary impact excitations show promising results for identification of frequency-dependent bearing coefficients. Suitable filtering of the shaft run-out and remnant imbalance are necessary for accurate identification of bearing coefficients. A time domain based run-out filtering algorithm is now available for application to impact excitation response measurements. Electro-magnetic actuators for improved control of the impacts are currently under construction.

TABLE OF CONTENTS

LIST OF TABLES

LIST OF FIGURES

Page

NOMENCLATURE

a	Cross-coupled to main stiffness ratio
B	System response matrix for mean square formulation
C	System damping matrix
c	Clearances for each type of element (bearing minimum radial clearance = 0.0762 mm, squeeze film damper radial clearance = 0.229 mm)
c_p, c_b	Journal bearing pad machined and assembled clearances (m)
C_{ij}, K_{ij}	Bearing-*ISFD* combined damping and stiffness coefficients, $i = x,y$, $j = x,y$ (N.s/m, N/m)
d_1, d_2	Distances from rotor CG to planes of imbalance (m)
E_{xy}, E_{yx}	Total relative error of parameter identification
e_{xy}, e_{yx}	Mean square error of parameter identification
E	Force vector from impact excitations
F	Imbalance force vector
f_1, f_2	Imbalance forcing functions applied at imbalance locations *1,2*
G	Gyroscopic moments system matrix
H	System matrix
I_T	Rotor total transverse moment of inertia (0.704 kg-m^2)
I_P	Rotor total polar inertia (0.299 kg-m^2)
j	$\sqrt{-1}$
K	System stiffness matrix
L	Axial length of each type of element (bearing = 22.9 mm, squeeze film damper = 23.0 mm)
l_1, l_2	Distances from rotor CG to bearing locations (m)
M	System mass matrix
m	Rotor mass (45.3 kg)
m_1, m_2	Imbalance masses attached at rotor middle disk (kg)
P	Vector of identified bearing parameters
Q	Matrix of rotor response to imbalance or impact excitations
q	Vector of response to imbalance or impact excitations
R	Land radius of bearing or damper (bearing = 15.08 mm, squeeze film damper = 48.26 mm)
r_1, r_2	Radii of disks where imbalance masses are attached (m)
r_p	Dimensionless journal bearing preload (0.405)
s_1, s_2	Distance from CG to location of proximity probes (m)
t	Time (s)
x,y	Coordinates or rotor motion at bearing locations, x: horizontal, y: vertical
x_p,y_p	Coordinates or rotor motion at probe locations, x: horizontal, y: vertical
ϕ_1, ϕ_2	Angular location of imbalance masses (degree)
μ	Viscosity of lubricant (ISO VG 10, Pa-s)
ξ_1, ξ_2	System damping ratios for cylindrical and conical modes
Ω	Rotor running speed (rad/s)
ω	Excitation frequency in impact tests (s^{-1})

$\omega_{n1,\ n2}$	System natural frequencies for cylindrical and conical modes (rad/s)

Subindexes

b	Refers to tilting pad bearing
d	Refers to integral damper

1. Introduction

Current trends in turbomachinery design demand higher power to weight ratios. These systems require flexible damped supports to safely traverse critical speeds and to reduce rotor eccentricity at midspan. Furthermore, there exists a demand for increased tolerance to imbalance and sudden loads for satisfactory engine performance, which accrue additional requirements to the rotor supports for vibration dissipation.

Tilting pad journal bearings (*TPJBs*) are customarily used in land-based gas turbine engines and compressors due to their inherent stability, long life and low power consumption. Recently, flexure pivot tilting pad journal bearings (*FPJBs*) have become popular due to their easiness of installation and reduced number of moving parts [1]. However, tilting pad bearings posses large oil film stiffness coefficients which inhibit damping mechanisms to properly dissipate vibration energy at the support locations. Introducing a flexible support in series with the tilting pad bearing allows to relocate critical speeds in rigid rotors and provides a means for extra amounts of viscous damping derived from a squeeze film damper (*SFD*).

Squeeze film dampers are mechanical elements used in aircraft gas turbines and process compressors to reduce vibration and forces transmitted from the rotating assembly into the supporting structure. The integral squeeze film damper (*ISFD*) recently advanced by Zeidan [2] provides advantages such as short axial length, light weight and easiness of installation. *ISFDs* provide satisfactory damping forces to rotor-bearing systems to safely traverse critical speeds [3].

Squeeze film dampers derive their performance from a lubricant being squeezed in the annular space between a non-rotating cylindrical journal and its housing. The journal, typically attached to the outer race of rolling element bearings, whirls due to the forces exerted by the rotor. The squeeze film action generates hydrodynamic pressures and therefore dissipative forces reacting to the applied external dynamic loads.

The objective of the current research is to advance an experimentally validated methodology for on site identification of stiffness and damping force coefficients in rotor-bearing systems. A test rigid rotor mounted on a series support (squeeze film damper-tilting pad journal bearing) will be used to carry out the proposed identification from measurements of imbalance response and transient excitations (impacts). A computational program will integrate force coefficients from the fluid film bearing and the squeeze film damper, and the experimental results will be compared to numerical predictions. The research will ultimately advance engineering recommendations for the best design of the series support and provide guidelines for the safe operation of bearings and dampers.

2. Bearing description

The test squeeze film damper is of the integral type with segmented films land in the circumferential direction. Figure 1 shows the geometry and main dimensions of the test element. The damper consists of an outer ring, 126 mm (4.961 in) in outer diameter with a circumferential groove for lubricant supply, and an inner ring (damper journal) on which a tilting pad bearing fits. Four pairs of S-shaped springs connect the outer and inner rings and a small clearance of 0.229 mm (9 mils) separates the two rings into four film lands (pads) where hydrodynamic pressure generates the damping forces. The clearance around the damper journal (in the film lands) is manufactured uneven so that the journal becomes centered under the springs' deflection due to the shaft weight. The damper film lands have an arc extent of 52°, axial length of 23 mm (0.906 in) and a radius of 48.15 mm (1.90 in). The inner ring originally accommodating ball bearings was recently modified to hold a tilting pad bearing.

The damper outer ring has four holes 1.6 mm (0.063 in) in diameter that serve as inlet lubricant ports to the squeeze film lands from the external groove. The inner ring has a lateral feeding port and an internal groove for oil supply into the tilting pad bearing. A flexible hose connection provides the lubricant to the tilting pad bearing through the damper journal from an independent supply line. Circumferential cover plates provide the means for sealing the damper ends thus enhancing the damping forces. In all tests planned, the dampers will operate with both ends open to ambient.

The connecting element between the *ISFD* and the test rotor is a four-pad, tilting pad bearing of the integral type (Figure 1). Table 1 details the main characteristics of the tilting pad bearing and the squeeze film damper. The calculated stiffness of the *TPJB* oil film is much larger than the integral damper spring stiffness (between 3.5 and 4.5 times at the rotor first critical speed of ~3,000 rpm) so that the rotor critical speed is largely governed by the *ISFD* stiffness and the support (pedestal) flexibility. In the planned experiments, the tilting pad bearings are fed with pure lubricant oil at all times and run under the same supply pressure of 12 psig (0.816 bars).

3. Past Relevant Literature

Conventional Tilting Pad Journal Bearings (*TPJBs*) offer the distinctive advantage over fixed geometry bearings of suppressing the cross coupled forces in the lubricant film that cause destabilizing effects [4]. On the other hand, *TPJBs* are very sensitivity to pad geometry variations (due to load and temperature-induced pad deformations), and to stacking of manufacturing tolerances that greatly affect their steady state and dynamic performance characteristics [5]. The modern manufacturing process Electro Discharge Machining (*EDM*) enables the pads to be integral to the bearing housing substituting the pad pivot element by thin flexible beams (webs) attaching the pads to the bearing housing and eliminating manufacturing limitations (tolerances) and pivot wear and fretting of conventional *TPJ* bearings.

In general, tilting pad bearings demonstrate their ability as stable support elements. However, the reduced damping forces due to thermal effects [6], pad elastic deformations [7], and pivot flexibility [8] among others, as well as large stiffness coefficients limit their application in turbomachinery where vibration dissipation is a crucial need. An external source of damping and a means for controlling (reducing) the support stiffness are desirable in order to accurately locate critical speeds and to reduce force transmissibility. Zeidan [2] incorporates squeeze film damper (*SFD*) supports in series with *FPJBs* to stabilize marginally stable rotors operating on *TPJB*s and where the sources of instability arise from mechanical components such as seals, impellers, blades and others.

Wire electrical discharge machining (*EDM*) also enables the manufacturing of integral squeeze film dampers (*ISFDs*) as shown schematically in Figure 1. The cylindrical journal of conventional dampers is replaced by a set of arquate segments (pads), their number depending on the particular application. Thin structural webs (springs) provide the support flexibility and attach the inner and outer rings. The thin gap between the sector pads and the outer ring forms the squeeze film lands. Each pad can be manufactured with different clearances to counter the static deflection due to the rotor weight. Additionally, the damper can be split for easiness of installation and retrofit. Zeidan [2] discusses successful applications of *ISFDs* in the petrochemical industry.

The reduced effective extent of the film lands in *ISFDs* affects its damping capacity as compared to conventional dampers. De Santiago et al. [9] present experiments on integral squeeze film dampers (*ISFDs*) supporting a three disk rigid rotor and subjected to rotating loads induced by calibrated imbalance masses. Measurements of the rotor synchronous response demonstrate the ability of the *ISFDs* in attenuating rotor vibrations in the range of operation from zero to 10,000 rpm. De Santiago and San Andrés [3] report further experiments with *ISFDs* incorporating end plate seals with calibrated clearances to enhance the damping capability of the test dampers. The particular construction of the centering springs enables the damper to consistently provide increasing damping coefficients for tighter seals and without a severe reduction in the through flow of lubricant to the damper land. This enables the *ISFD* to provide larger amounts of damping without excessive increments in the lubricant temperature.

Several applications of the bearing *SFD-TPJB* combination have been implemented in industry. De Santiago and San Andrés [10] present measured imbalance responses of a rigid rotor supported on this bearing combination. The bearing pair is effective in controlling amplitudes of vibration through the critical speeds (cylindrical and conical modes) with satisfactory transmissibility and engineered location of critical speeds. The response of rotor is shown to be also predictable with current analytical tools. The bearing combination is capable of taking dynamic loads up to five times the rotor weight as a result of the imbalance forces at maximum rotor speed.

Although current analytical models of the flow in *FPJBs* and *ISFDs* allow accurate prediction of dynamic force coefficients in most instances, it is sometimes necessary (desirable) to verify the magnitude of the bearing rotordynamic force coefficients in-situ.

Imbalance response measurements are ideal for identification of effective synchronous bearing coefficients once the rotor is in place and operating.

4. Identification of synchronous force coefficients using imbalance response measurements

The dynamics of a rigid rotor supported on two (different) anisotropic bearings are modeled as a four-degree of freedom system as the rotor traverses the first and second critical speeds corresponding to the cylindrical and conical modes of vibration [11]. Figure 2 details the rotor configuration on its bearing supports and appropriate dimensions. The derivation of the identification procedure begins with the equations of motion of the rotor-bearing system,

$$M\,\ddot{q} + C\,\dot{q} + \Omega G\,\dot{q} + K\,q = Fo\,e^{j\Omega t} \tag{1}$$

where M, C, and K are the (4x4) inertia, damping and stiffness matrices and G is the gyroscopic moments matrix given below. $F = Fo\,e^{j\Omega t}$ is the excitation force vector derived from imbalance masses attached at two planes along the rotor, and q is a vector containing the response of the rotor *at* the bearing locations $(1,2)$ and in two orthogonal directions (x, y) i.e.

$$q = [x_1, x_2, y_1, y_2]^T \tag{2}$$

In equation (1) Ω is the rotor speed, $j = \sqrt{-1}$, and t is time.

The inertia, damping, stiffness and gyroscopic matrices are given by:

$$M = \frac{1}{L}\begin{bmatrix} ml_2 & ml_1 & 0 & 0 \\ 0 & 0 & ml_2 & ml_1 \\ -I_T & I_T & 0 & 0 \\ 0 & 0 & I_T & -I_T \end{bmatrix} \quad C = \begin{bmatrix} Cxx_1 & Cxx_2 & Cxy_1 & Cxy_2 \\ Cyx_1 & Cyx_2 & Cyy_1 & Cyy_2 \\ -Cxx_1l_1 & Cxx_2l_2 & -Cxy_1l_1 & Cxy_2l_2 \\ Cyx_1l_1 & -Cyx_2l_2 & Cyy_1l_1 & -Cyy_2l_2 \end{bmatrix}$$

$$K = \begin{bmatrix} Kxx_1 & Kxx_2 & Kxy_1 & Kxy_2 \\ Kyx_1 & Kyx_2 & Kyy_1 & Kyy_2 \\ -Kxx_1l_1 & Kxx_2l_2 & -Kxy_1l_1 & Kxy_2l_2 \\ Kyx_1l_1 & -Kyx_2l_2 & Kyy_1l_1 & -Kyy_2l_2 \end{bmatrix} \quad G = \frac{1}{L}\begin{bmatrix} 0 & 0 & 0 & 0 \\ 0 & 0 & 0 & 0 \\ 0 & 0 & -I_P & I_P \\ -I_P & I_P & 0 & 0 \end{bmatrix} \tag{3}$$

where m is the rotor mass, I_T and I_P are the rotor transverse and polar inertia, $l_{1,2}$ is the axial distance from the rotor c.g. to each bearing location, and L is the bearing span. $(C_{ij})_{1,2}$ and $(K_{ij})_{1,2}$ are the bearing synchronous damping and stiffness coefficients at

locations 1 and 2. Note that the first two equations of motion correspond to conservation of linear momentum, whilst the last two equations relate to conservation of angular momentum in the rotor.

The generalized imbalance vector (Fo) in equation (1) is defined as:

$$Fo = \begin{bmatrix} f_1 + f_2 \\ -j(f_1 + f_2) \\ -f_1 d_1 + f_2 d_2 \\ -j(f_1 d_1 - f_2 d_2) \end{bmatrix} \Omega^2 \tag{4}$$

where the imbalance forcing functions f_1 and f_2 are

$$f_1 = m_1 r_1 e^{-j\phi_1} \text{ and } f_2 = m_2 r_2 e^{-j\phi_2} \tag{5}$$

with m_1 and m_2 as the imbalance masses attached at radii r_1 and r_2 and at circumferential locations ϕ_1 and ϕ_2, respectively.

At steady state, the rotor response is of the form $q = q_o e^{j\Omega}$, with the components of q_o being complex numbers. Thus, equation (1) reduces to:

$$j\Omega C q_o + K q_o = Fo + [\Omega^2 M - j\Omega^2 G] q_o \tag{6}$$

The bearing support reaction forces in the left hand side of equation (6) can be expressed as the product of a (4x16) response matrix Q, composed of linear combinations of the response vector (q_o), and a vector of system (synchronous stiffness and damping) parameters P (16x1) as:

$$Q P = j\Omega C q_o + K q_o \tag{7}$$

where:

$$Q = \begin{bmatrix} q_o^T & 0_V & jq_o^T & 0_V \\ 0_V & q_o^T & 0_V & jq_o^T \\ q_o^T l & 0_V & jq_o^T l & 0_V \\ 0_V & -q_o^T l & 0_V & -jq_o^T l \end{bmatrix}_{4x16} \quad l = \begin{bmatrix} -l_1 & 0 & 0 & 0 \\ 0 & l_2 & 0 & 0 \\ 0 & 0 & -l_1 & 0 \\ 0 & 0 & 0 & l_2 \end{bmatrix}, \tag{8}$$

and

$$P = [Kxx_1, Kxx_2, Kxy_1, Kxy_2, Kyx_1, Kyx_2, Kyy_1, Kyy_2, \\ \Omega Cxx_1, \Omega Cxx_2, \Omega Cxy_1, \Omega Cxy_2, \Omega Cyx_1, \Omega Cyx_2, \Omega Cyy_1, \Omega Cyy_2]^T_{16x1} \tag{9}$$

with 0_V representing a (1x4) zero vector.

Equation (6) is rewritten as

$$Q\,P = Fo + [\,\Omega^2 M - j\Omega^2 G\,]\,q_o \tag{10}$$

Separating real and imaginary parts of the complex equation (10) renders an undetermined system of 8 (real) linear algebraic equations to identify 16 rotordynamic coefficients representing the two anisotropic support bearings. A second set of imbalances (set B) generating linearly independent responses then completes the required number of equations to solve (10) for the vector of parameters P, i.e.

$$P = \overline{\overline{Q}}^{-1}\,\overline{\overline{F}}_T\,; \tag{11}$$

where $\overline{\overline{Q}} = \begin{bmatrix} \overline{Q}_A \\ \overline{Q}_B \end{bmatrix}$, $\overline{Q} = \begin{bmatrix} Re[Q] \\ Im[Q] \end{bmatrix}$, $\overline{\overline{F}}_T = \begin{bmatrix} \overline{F}_{TA} \\ \overline{F}_{TB} \end{bmatrix}$, $\overline{F}_T = \begin{bmatrix} Re[F_T] \\ Im[F_T] \end{bmatrix}$ (12.a)

and $$F_T = Fo + [\,\Omega^2 M - j\Omega^2 G\,]\,q_o \tag{12.b}$$

The condition for linear independence of the response matrix is easily obtained from the solution of equation (6) for the response vector q_o as:

$$q_o = H^{-1}(\Omega)\,Fo \tag{13}$$

where $$H(\Omega) = -\Omega^2 M + j\Omega^2 G + j\Omega C + K \tag{14}$$

Two linearly independent (l.i.) excitations Fo_A and Fo_B thus generate l.i. responses q_{oA} and q_{oB}. The conditions for linearly independent excitations can be stated from the definition of the excitation vector Fo, equation (3), i.e. the excitation in test B is l.i. from that of test A by changing the location and/or magnitude of the imbalance masses (m_1, m_2) at the two unbalance locations and such that the resultant vector Fo_B is not a (complex) multiple of the original vector Fo_A. Notice that excitations in only one imbalance plane could not render linearly independent excitation vectors since Fo_B can be expressed as a multiple of Fo_A. Thus, two imbalance planes are mandatory for identification of all 16 bearing parameters.

Lee and Hong [11] estimate speed-dependent synchronous bearing coefficients from equation (7) by separating the forward and backward whirl vibration responses resultant of the gyroscopic moments. However, this procedure is not necessary since the measured vibration q_o already contains the forward and backward whirl components. Thus, filtered synchronous vibration data is perfectly suitable, making the identification procedure easy to implement from running machine data in the field. Note that the analysis shows that two imbalance runs (A and B) are necessary in order to identify all force coefficients from two anisotropic bearings. Force coefficients from isotropic bearings will cause numerical

singularities during the inversion of the response matrix $\overline{\overline{Q}}$. The stated procedure is not able to identify the force coefficients in this case.

Tieu and Qiu [12] also identify sixteen synchronous coefficients of two different bearings supporting a rigid rotor from two or more imbalance response measurements. Tieu and Qiu utilize unfiltered responses and forward a numerical procedure to minimize noise influence. The experimental results show good correlation with theoretical predictions of force coefficients for a cylindrical journal bearing. The current identification procedure, on the other hand, can use filtered synchronous responses, and is therefore not affected by (high frequency) noise from the measurements. Modern data acquisition systems typically remove shaft run out from the measured signals using the tachometer reference. Thus this false vibration synchronous magnitude is not likely to perturb the method either.

The developed methodology is also suitable for implementation of redundant data, i.e. a least square formulation can be easily implemented if additional imbalance response measurements are available. Recall that with two imbalance runs and real and imaginary parts separated, the equations of motion lead to:

$$\overline{\overline{Q}}\,P=\overline{\overline{F}}_T=\overline{\overline{F}}o+[\,\overline{\overline{M}}-j\overline{\overline{G}}\,]\,\Omega^2\,\overline{\overline{q}}_o; \tag{15}$$

which is a system of 16 equations with 16 unknowns, and $\overline{\overline{Q}}$ represents a *set* of two linearly independent runs. If there are more than two recorded l.i. imbalance responses available, it is convenient to stack all responses (i.e. imbalance sets A and B, sets A and C, sets B and C, etc) as:

$$\begin{bmatrix} \overline{\overline{Q}}_1 \\ \overline{\overline{Q}}_2 \\ \cdot \\ \cdot \\ \cdot \\ \overline{\overline{Q}}_n \end{bmatrix} P = \begin{bmatrix} \overline{\overline{F}}_{T1} \\ \overline{\overline{F}}_{T2} \\ \cdot \\ \cdot \\ \cdot \\ \overline{\overline{F}}_{Tn} \end{bmatrix} \tag{16}$$

which can be written in compact form as:

$$B\,P=F \tag{17}$$

Finally, the least square formulation for this over-determined system (with more observations than parameters to be found) is:

$$P=(B^T\,B)^{-1}\,B^T\,F \tag{18}$$

Recall that $\overline{\overline{Q}}_i$ is formed from all possible combinations of imbalance sets, and that the condition for appropriate identification is that all tests are l.i. from each other. Permutations are avoided since the order in which the information is stacked is not relevant.

Finally, if measurements of the rotor response are not taken at the bearing locations l_1 and l_2, a simple geometrical transformation using the assumption of rigid rotor motion allows the use of imbalance responses x_{p1}, x_{p2} at locations s_1 and s_2 away from the rotor center of gravity (see Figure 2):

$$\begin{bmatrix} x_1 \\ x_2 \end{bmatrix} = \frac{1}{(s_1+s_2)} \begin{bmatrix} (l_1+s_2) & (s_1-l_1) \\ (s_2-l_2) & (l_2+s_1) \end{bmatrix} \begin{bmatrix} x_{p1} \\ x_{p2} \end{bmatrix} \tag{19}$$

Identification of synchronous coefficients from numerical predictions of imbalance response.

Numerical predictions of imbalance response of the test rotor allow identification of synchronous bearing coefficients over the rig operating range of speeds (100-10,000 rpm). Table 2 shows a summary of the mass, inertia and geometry characteristics of the test rigid rotor described in [10]. Table 3 summarizes the distribution of masses of four imbalance sets *A* through *D* used to generate dynamic responses. Note that all four imbalance combinations are linearly independent from each other as required by the identification procedure.

Table 4 shows (assumed) bearing synchronous stiffness and damping coefficients that remain constant throughout the identification speed range. The magnitude of these coefficients resembles previously calculated coefficients [3] so that the location of the critical speeds is not markedly different from that of the expected experimental observations [10]. The choice of constant force coefficients is useful to assess the accuracy and robustness of the identification procedure.

Table 5 shows the resulting (speed-dependent) damped natural frequencies and damping ratios of the rotor system as calculated from an eigenanalysis considering constant bearing stiffness and damping force coefficients. Gyroscopic effects are included in the calculations. Notice that the two rigid-body modes (cylindrical and conical) of vibration fall within the rotor operating range. Also note that the conical motions (second natural frequency) are more damped than the cylindrical mode.

Figure 3 shows numerical predictions of the rotor response (amplitude and phase) at the bearing locations, i.e. $s_1 = l_1$ and $s_2 = l_2$ using equation (13). The predictions shown are for imbalance masses and locations given in Table 3 as tests *A* and *B* respectively. Note that test *A* excites the first mode of vibration (cylindrical), whereas imbalance distribution *B* excites both modes of vibration (cylindrical and conical). Thus, for imbalance response *B*, two phase shifts are clearly identified, rendering a total phase shift in excess of 360°

past the second critical speed. Conical motion is evident by examining the phase angle between x_1 and x_2 locations at 7,000 rpm and observing a difference of ~ 180° for this test (B). Calculated motions at the first critical speed for the given imbalances are in the order of 20 to 25 % (60 - 80 microns 0-pk) of the total bearing clearance, and which in real applications should not compromise the assumption of small amplitude motions for rotordynamic force coefficients.

The imbalance responses from all mass distributions shown in Table 3 are supplied to the developed identification algorithm. Figure 4 depicts the estimated synchronous bearing coefficients. The identification procedure renders poor results at low speed ratios ($\omega/\omega_{n1} < 0.6$, i.e speeds lower than 2,000 rpm for this example) mainly due to the smallness of the response in this range of speeds (see Figure 3). Amplitudes of vibration are less than 8 % (5 microns pk-pk) of the maximum amplitude of vibration at the first critical speed (~ 60 microns pk-pk).

Prior to the first critical speed (between 2,000 and 3,000 rpm) there is a region in which the identification procedure renders improved results. The phase angle of the response begins a rapid change with still relatively small amplitudes of vibration in this range of speeds, and which may contribute to the distortion of the identified parameters. Past 3,000 rpm and up to 6,000 rpm, the identification is flawless in all 16 parameters. It is thus evident that the best identification range is located between the critical speeds. Identification of parameters is slightly distorted above 6,000 rpm, mainly for the cross-coupled stiffnesses (due to their smallness, as will be shown later).

Cross-coupled bearing stiffness coefficients are well known sources of instability in high-speed turbomachinery. A special study aims to assess the sensitivity of the identification procedure to the magnitude of the cross-coupled stiffness coefficients. The sensitivity study is based on the measure of the total (cumulative) relative error (E_{xy}, E_{yx}) of identified cross-coupled coefficients over a range of speeds as a function of the cross-coupled to main stiffness ratio (a) defined as

$$a = \frac{K_{ij}}{K_{ii}} \tag{20}$$

with $K_{ij} = \sqrt{(\overline{K}_{xy}^{\,2} + \overline{K}_{yx}^{\,2})/2}$ as a squared average and $K_{ii} = (\overline{K}_{xx} + \overline{K}_{yy})/2$ the average of stiffness in the main directions. The bars on the coefficients denote the arithmetic average of the values of stiffness in both supports (bearings 1 and 2). The definition of the cross-coupled to main stiffness ratio (a) is based in the assumption that the main stiffnesses along both directions (x,y) are not largely different. The squared average of the cross-coupled coefficients aims to avoid reduction to zero of the K_{ij} term in case the coefficients are of the same magnitude and opposite in sign (i.e. maximum destabilizing effect).

The mean square error e_{xy}, over the speed range of identification is:

$$e_{xy} = \frac{1}{n}\sqrt{\sum_{i}^{n}(\hat{K}_{xy_i} - K_{xy_i})^2} \tag{21}$$

where n is the number of identification steps and the ($\hat{}$) on the K_{xy} term indicates the identified parameters with K_{xy} as the actual value at the given speed. A similar definition applies for the cross-coupled coefficients K_{yx}. The total relative error E_{xy} then becomes:

$$E_{xy} = \frac{e_{xy}}{K_{xy}} \tag{22}$$

A similar definition follows for E_{yx}.

A parametric study for different values of cross-coupled to stiffness ratio (a) serves to assess the goodness of the identification procedure for the cross-coupled stiffness coefficients. The relative magnitude coefficient a varies from 1.3% (current value in numerical example) to 100% (with intermediate values equal to 2, 5, 10, and 50%). Figure 5 summarizes these results and shows that the total relative error drops significantly for values of the relative magnitude coefficient (a) larger than 2%, with a total relative error of less than 10% and remaining almost constant for larger values of the relative magnitude coefficient (a). The comparisons are based on an equal number of samples n within the identification range since this also affects the magnitude of the total relative error, in particular for the case in which there exist excessive samples in the low speed range.

The (numerical) identification procedure shows that most of the total relative error comes from poor identification at low speeds due to the smallness of the rotor response. It is thus possible to conclude that the identification technique will render satisfactory results for the cross-coupled stiffness if the magnitude of these coefficients is larger than 2% of the direct stiffness, and if the amplitude of the synchronous response is larger than 8 % of the maximum amplitude of vibration at the first critical speed.

5. Identification of frequency-dependent force coefficients using impact response measurements

Tilting pad bearings possess linearized rotordynamic force coefficients that are dependent upon the frequency of rotor vibration [13]. In addition, the combined support *SFD-TPJB* shows frequency-dependent coefficients since the equivalent stiffness and damping coefficients result from a series impedance formulation. Thus, suitable procedures for parameter identification should render both synchronous and non-synchronous bearing coefficients.

Non-synchronous rotordynamic coefficients are of paramount importance for stability studies when asynchronous sources of excitation are known to be present in the system. Parsell et al. [14] demonstrate that subsynchronous rotordynamic force coefficients of

TPJBs remain almost constant at any frequency ratio (frequency/running speed) for the case of preloaded bearings. Non-preloaded bearings, however, present non-synchronous coefficients that can be substantially different from the synchronous coefficients. The general trend shows reduced damping coefficients and increased bearing stiffnesses as the frequency of excitation decreases. Ha and Yang [15] present experimental force coefficients of a zero-preloaded, five pad *TPJB* bearing using steady sinusoidal excitations from hydraulic shakers. Ha and Yang find that the frequency of excitation has little effect on the rotordynamic force coefficients for the test bearing considered. Stiffness coefficients slightly decrease as the excitation frequency ratio increases, while damping coefficients slightly increase.

Non-synchronous bearing stiffness and damping coefficients at any rotor speed can also be identified from the rotor response to transient excitations, due to impacts for example. This method has the advantage of exciting a whole range of frequencies in a single experiment if enough energy is delivered while impacting, thus considerably shortening the experimentation effort as compared with steady state periodic excitations. Additionally, impact excitations have the potential for in-situ identification of equivalent frequency-dependent bearing force coefficients.

The equations of motion of the rotor-bearing system for a perfectly balanced rotor are given by

$$M\ddot{q} + C\dot{q} + \Omega G\dot{q} + Kq = E(t) \tag{23}$$

with M, C, K, G and q as defined before, and $E(t)$ is the transient excitation (impact) force defined as

$$E(t) = \begin{bmatrix} \sum_i Fi_X \\ \sum_i Fi_Y \\ \sum_i d_i Fi_X \\ \sum_i d_i Fi_Y \end{bmatrix} \tag{24}$$

with $Fi_{X,Y}(t)$ as the excitation force (impact) applied at the i-th location along the rotor and at a distance d_i from the center of gravity. Notice that the stiffness and damping matrices are speed and frequency dependent, i.e. $C, K = f(\Omega, \omega)$. Equation (23) is written in the frequency domain as

$$M\ddot{q}(\omega) + C\dot{q}(\omega) + \Omega G\dot{q}(\omega) + Kq(\omega) = E(\omega) \tag{25}$$

and at any given frequency ω, $E(\omega) = Eo\, e^{j\omega t}$ and $q(\omega) = qo\, e^{j\omega t}$, with Eo nearly a constant for a perfect impact. Thus, equation (25) reduces to

$$-\omega^2 M q_o + j\omega\Omega G q_o + j\omega C q_o + K q_o = Eo \tag{26}$$

Note that equation (26) holds at any given rotor speed (Ω) and at any particular frequency (ω). Bearing forces can also be written as the product of a response matrix (Q) and a vector of parameters (P) and resolved in terms of the external excitation, gyroscopic and inertia terms as in equation (10) above. Separating real and imaginary parts, a system of 8 (real) algebraic equations can be written with 16 (frequency dependent) unknown parameters, in the same way as the identification procedure using imbalance responses dictates.

A second set (B) of excitations generating linearly independent responses then completes the required number of equations to solve for the parameters vector (P) as before. The conditions for the linear independence of the transient responses are easily inferred from the solution of equation (26) for (q_o) as:

$$q_o = H^{-1}(\Omega,\omega)\,Eo \tag{27}$$

where
$$H(\Omega,\omega) = -\omega^2 M + j\omega\Omega G + j\omega C + K \tag{28}$$

Two linearly independent excitations (Eo_A) and (Eo_B) thus generate *l.i.* responses (q_{oA}) and (q_{oB}), respectively. The conditions for linearly independent excitations can be stated from the definition of the excitation vector in equation (24), i.e. the excitation in test B is *l.i.* from that resulting in test A by simply shifting the excitation location along the rotor, or by exciting first in one direction and then in an orthogonal direction. Excitations may be applied at the rotor center of gravity or away from it.

Assuming the bearing coefficients to be identical on both sides of the rotor reduces the number of unknowns to 8, and the identification becomes possible with only one impact excitation. In all cases, several consecutive impacts at the same rotor speed provide redundant data for error minimization in the same way as for the imbalance response-based identification procedure. Measurements of the rotor response to impacts can also be conducted away from the exact bearing locations with the coordinate transformation given by equation (19).

Identification of frequency-dependent coefficients from numerical predicitions of system response to impact excitations.

Rotor response to impact excitations allows for identification of frequency-dependent bearing rotordynamic coefficients at a fixed rotor speed. Numerical predictions are performed for the test rotor with the characteristics listed in Table 2. The rotordynamic coefficients are held constant in the frequency range of study 2-200 Hz (120-12,000 cpm) to cover the operating range of speeds (0-10,000 rpm). The running speed is set to 1,000 rpm (17 Hz) to demonstrate that the identification methodology (theoretically) provides good results for synchronous coefficients even at low speeds.

Table 6 shows the magnitude in the frequency domain and location of ideal impacts for excitation of the rotor. These impacts represent the simplest (linearly independent) combination applied at a single axial location, vertical and horizontal directions.

Redundant data would be implemented just in the same manner as in the case of imbalance responses. Ideal impacts with a uniform load (~ 110 N) over a extended frequency range correspond to just 27% of the rotor weight and are applied at the rotor center of gravity for the current numerical experiment (constant within the identification range). Note that in the time domain, the loads required will amount to ~ 4,500 N (1,000 lbs) over a short time span of about 3.5 ms (typical of soft-tip impacts) to excite a frequency range of 100 Hz with a cut-off amplitude of 80%. Shorter impact times (harder-tip impacts, 1.6 ms typical) raise the cut-off frequency above 200 Hz but demand a larger impact load up to ~10,000 N (2,250 lb).

The rotordynamic bearing force coefficients used to generate the theoretical response are the same as for the case of imbalance response calculations and presented in Table 4. The coefficients are constant throughout the frequency range to better illustrate the goodness of the identification procedure.

Figure 6 shows the numerical responses (frequency response functions) at the bearing locations and for the two impacts. Note that impacts in the horizontal direction obviously produce larger motions in the horizontal direction with vertical motions only due to the cross-coupled forces. The magnitude of the applied force produces peak motions in the same direction as large as 30% of the bearing clearance as in the case of the imbalance response and at the estimated natural frequencies (see Table 5). Note that the phase angle of response in the orthogonal directions presents large shifts even though the impacts barely excite the conical mode in the main directions, so it is expected that the phase angle will have a strong influence in the identification of the cross coupled coefficients.

Finally, note that the effect of the running speed on the response is zero since the assumption is made of a perfectly balanced rotor i.e. the dynamic response at the synchronous speed is solely governed by the value of the synchronous coefficients and the magnitude of the impact force. In practice, both remnant imbalance and shaft run-out will have a strong influence on the dynamic response at the running speed, thus suitable procedures for subtraction of these effects have to be devised in order to correctly identify synchronous coefficients from impact excitations.

Figure 7 shows the identified frequency-dependent coefficients of the bearing elements at a fixed rotor speed of 1,000 rpm. All coefficients are meanly perfectly identified throughout the frequency range, with deviations from the theoretical values due to numerical rounding. Improved coefficient identification in the low frequency range in Figure 7 is explained by noting that that the amplitudes of response at low frequencies in the main directions (Figure 6) are sufficiently large as opposed to the amplitudes of response at low speed for the case of imbalance excitations. Notice also that the amplitudes of vibration in the crossed directions are very small, thus it is likely that these measurements will be affected by noise in real applications.

6. Test rig and current experimental progress

The test rig intended for the experimental measurements is the same apparatus used by De Santiago and San Andrés [10] in previous measurements of rotor imbalance response (see Figure 8). This rig features a rigid rotor that is well suited for the proposed identification and supported on two identical bearings with series *FPJBs* and integral *SFDs*. The rig rests on a base plate bolted to a heavy worktable standing on an elastomeric vibration-absorbing pad. A 7.5 kW (10 HP) DC power supply and DC motor drive the test rotor through a flexible coupling. A *drawn cup* roller clutch in the coupling allows the motor to bring the rotor to a top speed of 10,000 rpm and can be shut off without applying a torque to the freely rotating shaft. This feature of the coupling ensures free coast down tests of the rig as the motor friction drag barely affects the rotor deceleration rate. Appendix A presents a complete description of the test rotor, bearing pedestals, lubrication system and data acquisition system.

Currently, imbalance response measurements of the rotor supported on series *FPJBs* and integral dampers have been recorded as well as imbalance response measurements of the rotor supported on *FPJBs* alone. Recorded responses of rotor on *FPJBs* only are for two linearly independent sets of imbalance, whereas responses of rotor on *FPJBs* and *ISFDs* are for three l.i. sets of imbalance. Preliminary identification rendered poor results in both cases with bearing parameters varying with no defined trend mainly due to the effect of the pedestal vibration on the measurements of rotor motion. Specifically, variations in the phase angle of response seem to have a strong deleterious effect on the identification procedure.

Presently, it is mandatory to account for pedestal motions to improve the bearing parameter identification from imbalance response measurements. Accelerometers installed on the pedestals provide sufficient information for pedestal parameter identification, but additional degrees of freedom must first be introduced into the rotor-bearing model. Diaz and San Andrés [16] followed this approach for improved identification of damping coefficients of conventional squeeze film dampers using measurements of the rotor synchronous orbits.

Modifications to test rig for impact excitation mechanism

Imbalance response measurements require no further modifications to the existing facility. On the other hand, impact response identification does require adequate mechanisms for application of impulsive loads. Figure 9 shows the designed mechanism for this end, and whose construction is currently under way. The impactor consists of an electromagnetic actuator that drives a rod with a steel rolling element at the end so that this miniature ball bearing hits the rotor middle disk after the triggering electrical signal is sent to the actuator. A piezoelectric load cell connects the driving rod and the rolling element and measures the effective load applied to the rotor. Two pre-loaded springs return the rod to its resting position after the impact. The distance between the rolling element and the rotor disk is set to a minimum to avoid inertia forces and rattling of the

impactor elements. The test fixture provides slots for alignment of the rod so that the impact is always directed in the radial direction of the rotor disk.

Currently, the impact mechanism is complete except for the electromagnetic actuator. The electromagnetic actuators will be acquired shortly. Preliminary impact tests with a calibrated hammer show good excitation for rotor speeds of zero, 2,000, 2,800 and 4,000 rpm. Typical impact duration is in the order of 0.002 s exciting a frequency range of over 300 Hz, i.e. about 4.5 times the maximum rotor running speed of 4,000 rpm. Largest dynamic motions are in the order of 127 microns in the direction of impact, i.e. about 40% of the combined bearing (*ISFD + FPBJ*) radial clearance.

A time-based algorithm for shaft run-out filtering is also ready at this time. The procedure consists of taking a full cycle of rotor motion in the four locations of measurement and subtracting this signature (false vibration or shaft run-out) from the dynamic signal recorded after the impact. A suitable timing obtained from the tachometer signal is necessary for this operation. The effect of the impact typically lasts for 5 (low speeds) to 20 (high speeds) revolutions of the rotor shaft.

Experimental time-filtered data results in frequency responses (FFT signatures) that show small amplitudes at the running speed (synchronous frequency). This component comes from to the impact itself, small remnant imbalance and numerical stack-up due to the compensation procedure. This last source is markedly evident in the spectrums of the crossed direction motions.

7. Closure

This report details the progress on the parameter identification of the integral squeeze film damper-tilting pad bearing series support of the NSF-SFD test rigid rotor. Two suitable methodologies are presented for this end, namely identification from imbalance response measurements and from impact response measurements. Imbalance response measurements provide information for identification of synchronous force coefficients whereas impact responses allow for identification of frequency-dependent bearing parameters.

The condition for identification of bearing coefficients for the case of imbalance response measurements is that at least two linearly independent responses at four locations (two bearing locations, two orthogonal directions) are necessary. Trial imbalance masses must be located such that the excitation vectors are independent from each other in the two tests. Parameter identification from impact excitation requires at least two impacts on the rotor at the same speed. Impacts can be performed in the same direction at two different axial locations or at the same location but in two orthogonal directions. Both methods lend themselves to a least square formulation in case redundant data are available.

The numerical simulations presented show that identification from imbalance responses is adequate for rotor speeds above 60% of the first rigid rotor critical speed due to the smallness of the response at lower speeds. The experiments also show that the best identification range is between critical speeds. Identification of cross-coupled stiffness requires that the relative magnitude of these coefficients with respect to the main stiffness coefficients is larger than 2%.

Preliminary experiments for identification of bearing parameters from imbalance responses show poor results mainly due to the motion of the (flexible) pedestals. It is necessary to include additional degrees of freedom into the identification procedure to account for the pedestal motions.

Experimental vibration signatures from preliminary impact excitations show promising results for identification of frequency-dependent bearing coefficients. Suitable filtering of the shaft run-out and remnant imbalance are mandatory for accurate identification of coefficients and mainly at the synchronous frequency. Use of a synchronous (tracking) filter could sweep away the response at the running speed considerably altering the response spectrum. Remnant imbalance contribution must also be taken into account for correct identification of synchronous coefficients. Run-out filtering in time domain is now available and shows good results. Electro-magnetic actuators for improved control of the impact excitations are currently under construction.

A sensitivity study is pending for both identification methods, and in particular for changes in the phase angle of vibration, as commonly encountered in practice as a result of the interaction of the rotor motions with the support vibration.

Finally, integration of existing *SFD* and *TPJB* force coefficients predictive codes into a single program should render equivalent bearing coefficients of the series support for comparison to the experimental values. The *SFD* program currently available solves the Reynolds equation of lubrication for isothermal, incompressible fluids with appropriate boundary conditions using Finite Elements [17]. The *TPJB* program renders rotordynamic force coefficients from the solution of the bulk-flow equations on each bearing pad [18]. Equivalent force coefficients are then assembled in an equivalent impedance formulation derived from the equations of motion of the support elements. The integrated program should run in a Windows Excel interface, whereas the equivalent impedance calculations will be programmed in Fortran.

8. Acknowledgements

The support of the TAMU Turbomachinery Consortium and the partial support of the National Science Foundation are gratefully acknowledged.

9. References

[1] De Choudhury, P., Hill, M. R., and Paquette, D. J., 1992, "A Flexible Pad Bearing System for a High Speed Centrifugal Compressor", *Proceedings of the 21st Turbomachinery Symposium*, Dallas, TX, pp 57-64.

[2] Zeidan, F., 1995, "Application of Squeeze Film Dampers", *Turbomachinery International*, Vol. 11, September/October, pp. 50-53.

[3] De Santiago, O., and L. San Andrés, 1999, "Imbalance Response and Damping Force Coefficients of a Rotor Supported on End Sealed Integral Squeeze Film Dampers", ASME Paper No. 99-GT-203.

[4] Hagg, A. C., 1946, "The Influence of Oil-Film Journal Bearings on the Stability of Rotating Machines", Transactions of the ASME, *Journal of Applied Mechanics*, Vol. 68, Sept., pp. A211-A220.

[5] Zeidan, F. Y., and Paquette, D. J., 1994, "Application of High Speed and High Performance Fluid Film Bearings in Rotating Machinery", *Proceedings of the 23st Turbomachinery Symposium*, Dallas, TX, pp 57-64.

[6] Ettles, C. M. McC., 1980, "The Analysis and Performance of Pivoted Pad Journal Bearings Considering Thermal and Elastic Effects", Transactions of the ASME, *Journal of Lubrication Technology*, April, Vol. 102, pp. 182-192.

[7] Desbordes, H., Fillon, M., Wai, C. C. H., and Frene, J., 1994, "Dynamic Analysis of Tilting-Pad Journal Bearing - Influence of Pad Deformations", Transactions of the ASME, *Journal of Tribology*, July, Vol. 116, pp. 621-628.

[8] Kirk, R. G., and Reedy, S. W.,1988, "Evaluation of Pivot Stiffness for Typical Tilting-Pad Journal Bearing Designs", Transactions of the ASME, *Journal of Vibration, Acoustics, Stress, and Reliability in Design*, April, Vol. 110, pp. 165-171.

[9] De Santiago, O., J. Oliveras, and L. San Andrés, 1999, "Imbalance Response of a Rotor Supported on Open-Ends Integral Squeeze Film Dampers", *ASME Journal of Gas Turbines and Power*, Vol. 121, 4, pp. 718-724.

[10] De Santiago, O., and L. San Andrés, 2000, "Measurements of the Imbalance Response in a Rotor Supported on Tilting Pad Bearings and Integral Squeeze Film Dampers," Turbomachinery Research Consortium Annual Report, Texas A&M University, TRC-SFD-01-00, May.

[11] Lee, C. W., and S. W. Hong, 1989, "Identification of Bearing Dynamic Coefficients By Unbalance Response Measurements", Proc. Instn. Mech. Engrs., Vol. 203, pp. 93-101.

[12] Tieu, A. K., and Z. L. Qiu, 1994, "Identification of Sixteen Dynamic coefficients of Two Journal Bearings From Experimental Unbalance Responses", *Wear*, Vol. 177, pp. 63-69.

[13] Lund, J. W., 1964, "Spring and Damping Coefficients for the Tilting-Pad Journal Bearing", *ASLE Transactions*, Vol. 7, pp. 342-352.

[14] Parsell, J. K., P. E. Allaire, and Barrett, L. E., 1983, "Frequency Effects in Tilting Pad Journal Bearing Dynamic Coefficients", *ASLE Transactions*, Vol. 26, April, pp. 222-227.

[15] Ha, H. C., and S. H. Yang, 1998, "Excitation Frequency Effects on the Stiffness and Damping Coefficients of a Five-Pad Tilting Pad Journal Bearing" ASME paper No. 98-TRIB-44.

[16] Díaz, S. E., and L. San Andrés, 2000, "Orbit-Based Identification of Damping Coefficients For a Rotor Mounted on Off-Centered Squeeze Film Dampers and Including Support Flexibility" ASME Paper N. 2000-GT-394, May.

[17] San Andrés, L. and Vance, J., 1987, "Effect of Fluid Inertia on Finite Length Sealed Squeeze Film Dampers," *ASLE Transactions*, Vol. 30, No. 3, pp. 384-393.

[18] San Andrés, L., 1996, "Turbulent Flow, Flexure-Pivot Hybrid Bearings for Cryogenic Applications," Transactions of the ASME, *Journal of Tribology*, Vol. 118, 1, pp. 190-200.

TABLES

Table 1. Integral squeeze film damper and flexure pivot tilting pad bearing main dimensions and operating conditions.

Squeeze film damper:		
Damper land radius (R_d)	48.26 mm	1.900 in
Land radial clearance (c_d)	0.229 mm	0.009 in
(after static deflection under rotor weight)		
Damper axial length (L_d)	23.00 mm	0.910 in
Land arc extent (in circumferential direction, nom.)		52°
Flexure pivot tilting pad bearing: 4 pads (70°)		
Bearing nominal diameter:	30.15 mm	1.187 in
Bearing axial length: (L_b)	22.9 mm	0.902 in
Pad radial clearance: (c_p)	0.127 mm ± 0.005 mm	0.0050 in ± 0.00013 in
Pad preload: 0.405 (r_p)	0.0508 mm	2 mils
Pivot offset:	0.50	
Bearing radial clearance: (c_b)	0.076 mm	3 mils
Pad rotational stiffness:	40 N-m/rad	354 lb-in/rad
Clearance on back of pads:	0.178 mm (typ)	0.007 in (typ)
Average inlet lubricant viscosity (μ)	15.76 cP	at 24.4° C (76° F)
Operating speed range:	0-10,000 rpm	
Static load between pads		
Drive end bearing	247.3 N	55.53 lb (51.90 psi - specific load)
Free end bearing	198.2 N	44.50 lb (41.56 psi - specific load)

Table 2. NSF test rig rigid rotor properties for numerical example.

Units	*ISO*		*English*	
Rotor mass	41.7 kg		91.8 lb	
Rotor total mass (including half of flexible coupling) (m)	45.3 kg		99.8 lb	
Rotor total transverse moment of inertia (I_T)	0.704 kg-m^2		2406 lb-in^2	
Rotor total polar inertia (I_P)	0.299 kg-m^2		1022 lb-in^2	
	mm		in	
Shaft diameter	76.2		3.00	
Shaft diameter at bearing locations	29.997		1.181	
Total length	673.11		26.50	
Bearing span	406.4		16.00	
Rotor cg location from coupling end				
Distances from cg to bearing locations (l_1,l_2)	0.189	0.217	7.44	8.54
Distances from cg to planes of imbalance (d_1,d_2)	0.067	0.102	2.64	4.02
Radius of disks where imbalances are attached (r_1,r_2)	0.114	0.095	4.49	3.74
Distances from cg to planes of impact excitation	0	0	0	0
Distances from cg to location of proximity probes (s_1,s_2)	0.119	0.146	4.69	5.75

Table 3. Summary of imbalance mass locations for numerical response of test rotor.

Location	Test A	Test B	Test C	Test D
Drive end disk	3.3 gr at 0°	4.1 gr at 90°	3.3 gr at -90°	4.1 gr at 0°
Fee end disk	3.3 gr at 0°	5.1 gr at 0°	4.28 gr at -90°	5.1 gr at 90°

Drive end disk: radius $r_1 = 0.114$ m, distance from rotor CG $d_1 = 0.067$ m.
Free end disk: radius $r_2 = 0.095$ m, distance from rotor CG $d_2 = 0.102$ m.
Positive angles on rotor are measured opposite to direction of rotation and from rotating reference (i.e. keyway in rotor or reflective pick-up mark).

Table 4. Bearing parameters used to generate (synchronous) imbalance response (constant over the speed range) and response to ideal impacts (constant over a frequency range).

Bearing 1:

Stiffness coefficients (N/m)	Damping coefficients (N-s/m)
$K_{xx} = 3.0 \times 10^6$	$C_{xx} = 2{,}000$
$K_{yy} = 3.5 \times 10^6$	$C_{yy} = 2{,}200$
$K_{xy} = 5.0 \times 10^4$	$C_{xy} = 250$
$K_{yx} = 3.0 \times 10^4$	$C_{yx} = 800$

Bearing 2:

Stiffness coefficients (N/m)	Damping coefficients (N-s/m)
$K_{xx} = 3.0 \times 10^6$	$C_{xx} = 2{,}000$
$K_{yy} = 3.5 \times 10^6$	$C_{yy} = 2{,}200$
$K_{xy} = 5.0 \times 10^4$	$C_{xy} = 250$
$K_{yx} = 3.0 \times 10^4$	$C_{yx} = 800$

Table 5. Calculated damped natural frequencies and damping ratios of test rotor-bearing system with constant stiffness and damping coefficients (gyroscopic effects included).

Cylindrical	
$\omega_1 = 57.8$ Hz, 61.3 Hz (3467, 3676 cpm)	$\xi_1 = 0.114, 0.131$

Conical	
$\omega_2 = 83.3$ Hz (4997 cpm, backwards)	$\xi_2 = 0.201$
$\omega_2 = 123$ Hz (7360 cpm, forward)	$\xi_4 = 0.199$

Table 6. Impact planes and magnitude of loads (in frequency) for numerical experiment on dynamic response of rotor to impact excitations.

Experiment	Load, Plane 1 (N)	Load, Plane 2 (N)	Direction of load
Test A	120	0	Horizontal (x)
	0	0	Vertical (y)
Test B	0	0	Horizontal (x)
	100	0	Vertical (y)

Impact planes located at rotor C.G., i.e. $d_1 = d_2 = 0$ m.

FIGURES

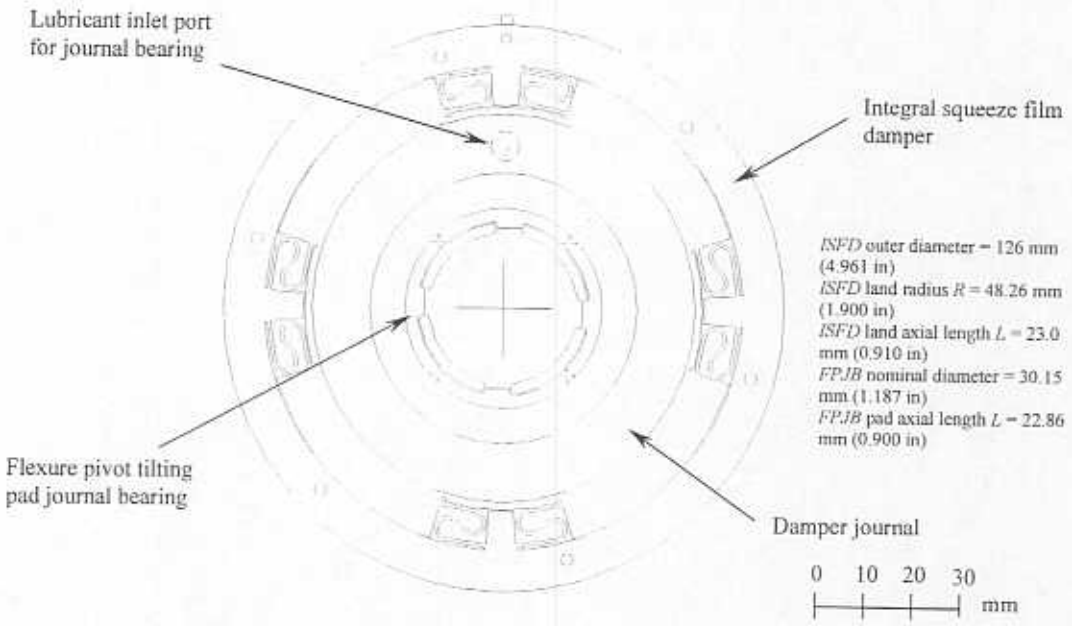

Figure 1. Integral squeeze film damper and flexure pivot tilting pad journal bearing assembly

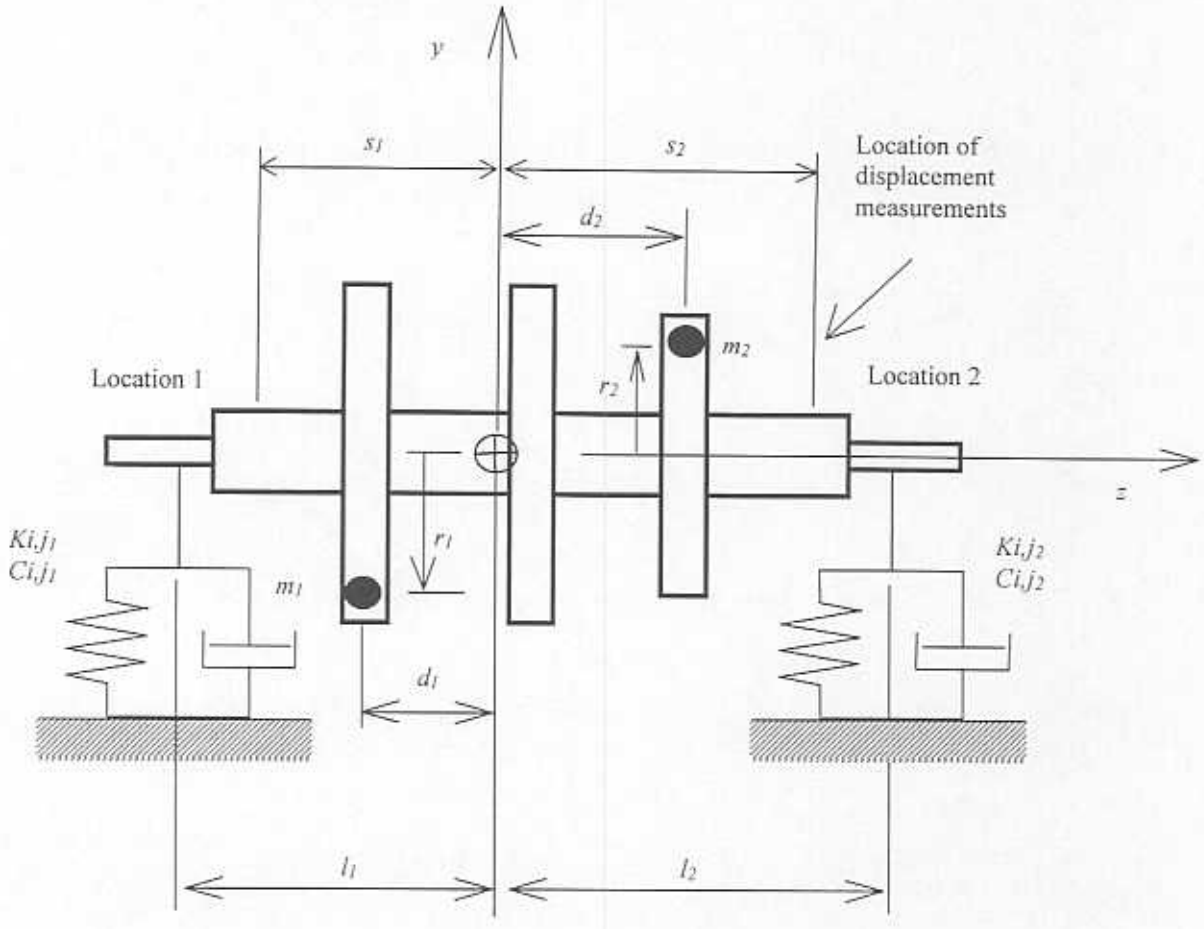

Figure 2. Rotor model for identification of equivalent support parameters.

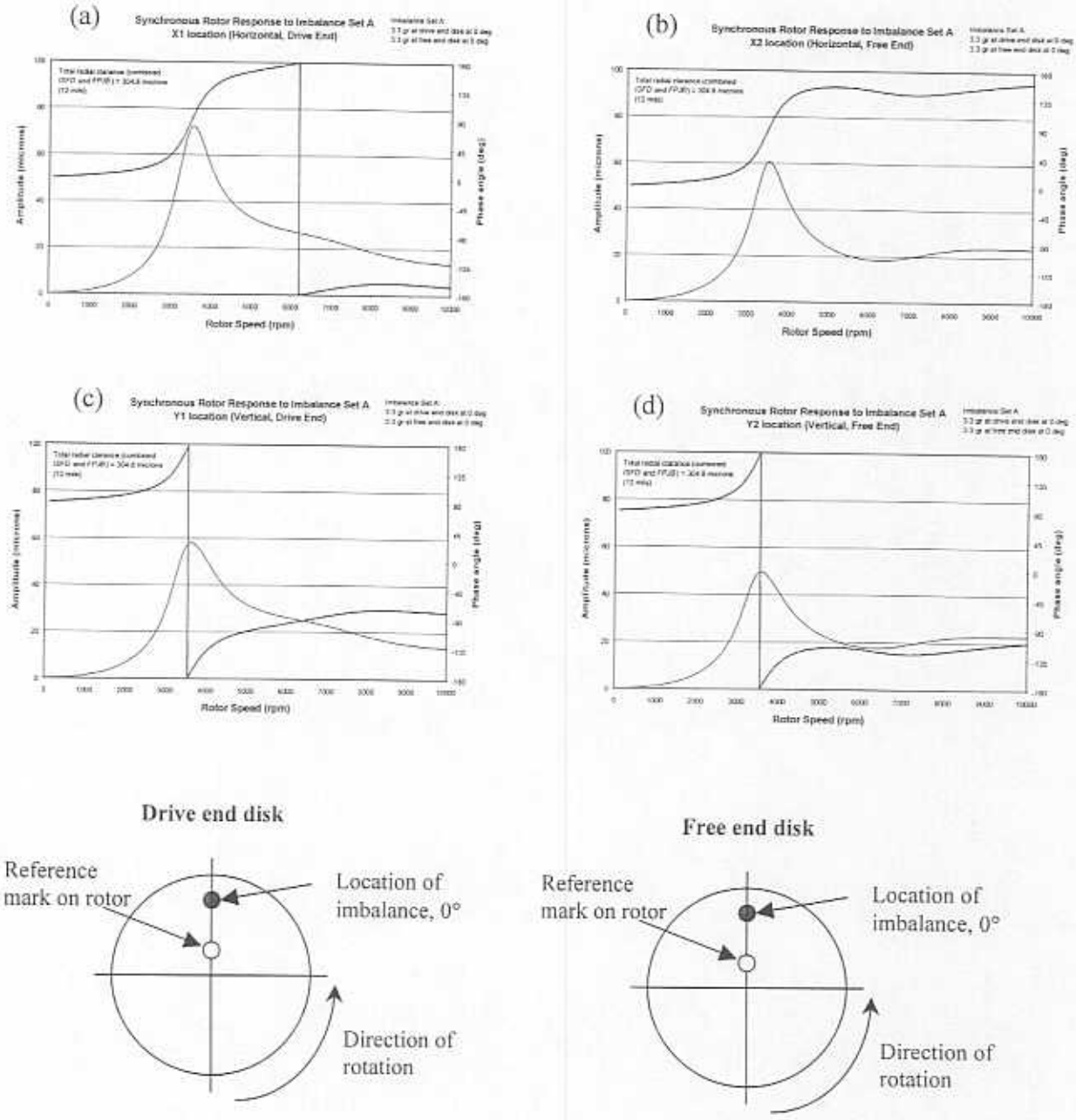

Figure 3a. Predicted imbalance response (magnitude and phase) of rigid rotor to imbalance set A at bearing locations. (Drive end disk radius = 0.114 m, d1 = 0.067m, free end disk radius = 0.095m, d2 = 0.102m). (a) Drive end, horizontal, (b) Free end, horizontal, (c) Drive end, vertical, (d) Free end, vertical)

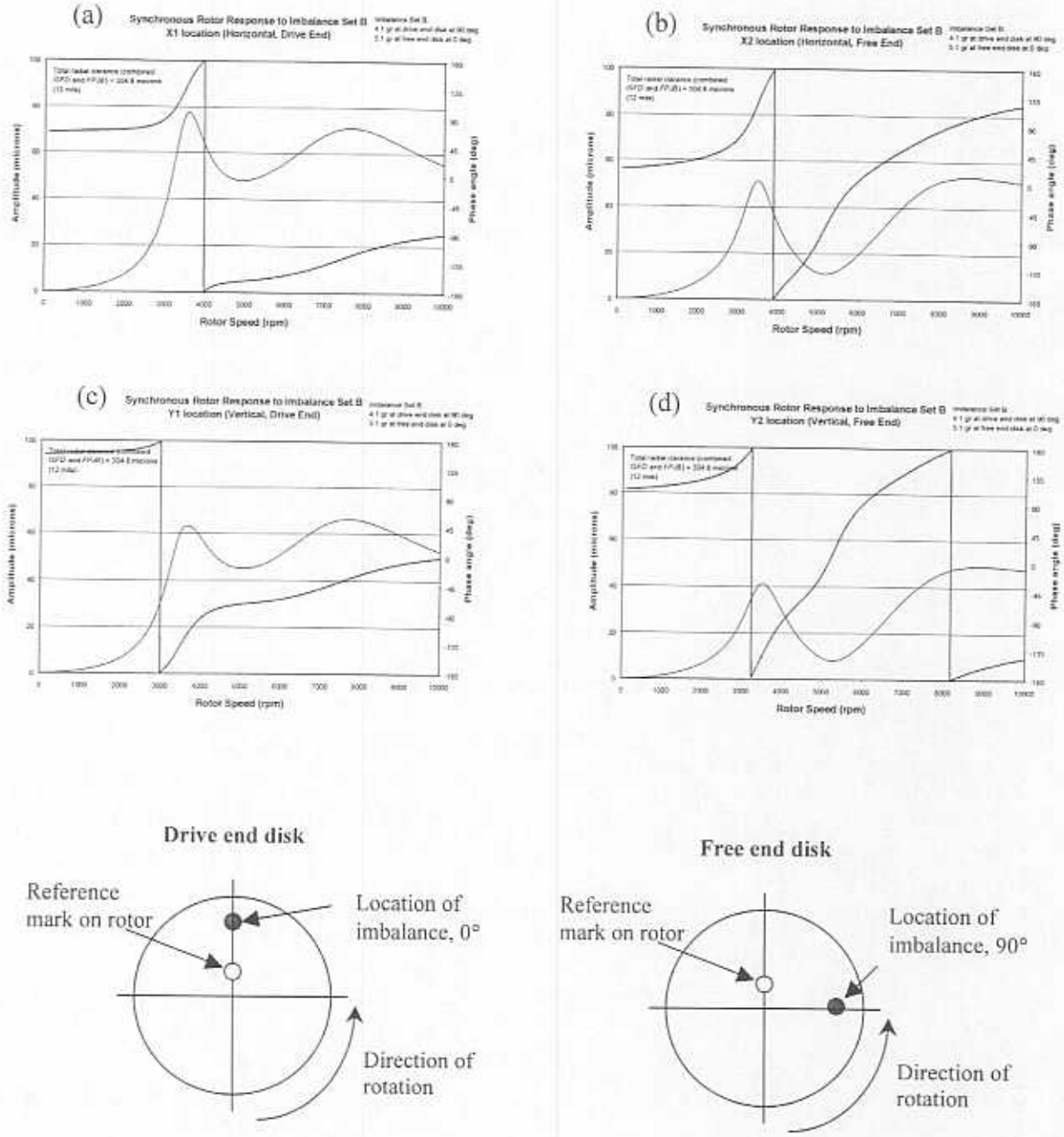

Figure 3b. Predicted imbalance response (magnitude and phase) of rigid rotor to imbalance set B at bearing locations. (Drive end disk radius = 0.114 m, d1 = 0.067m, free end disk radius = 0.095m, d2 = 0.102m). (a) Drive end, horizontal, (b) Free end, horizontal, (c) Drive end, vertical, (d) Free end, vertical)

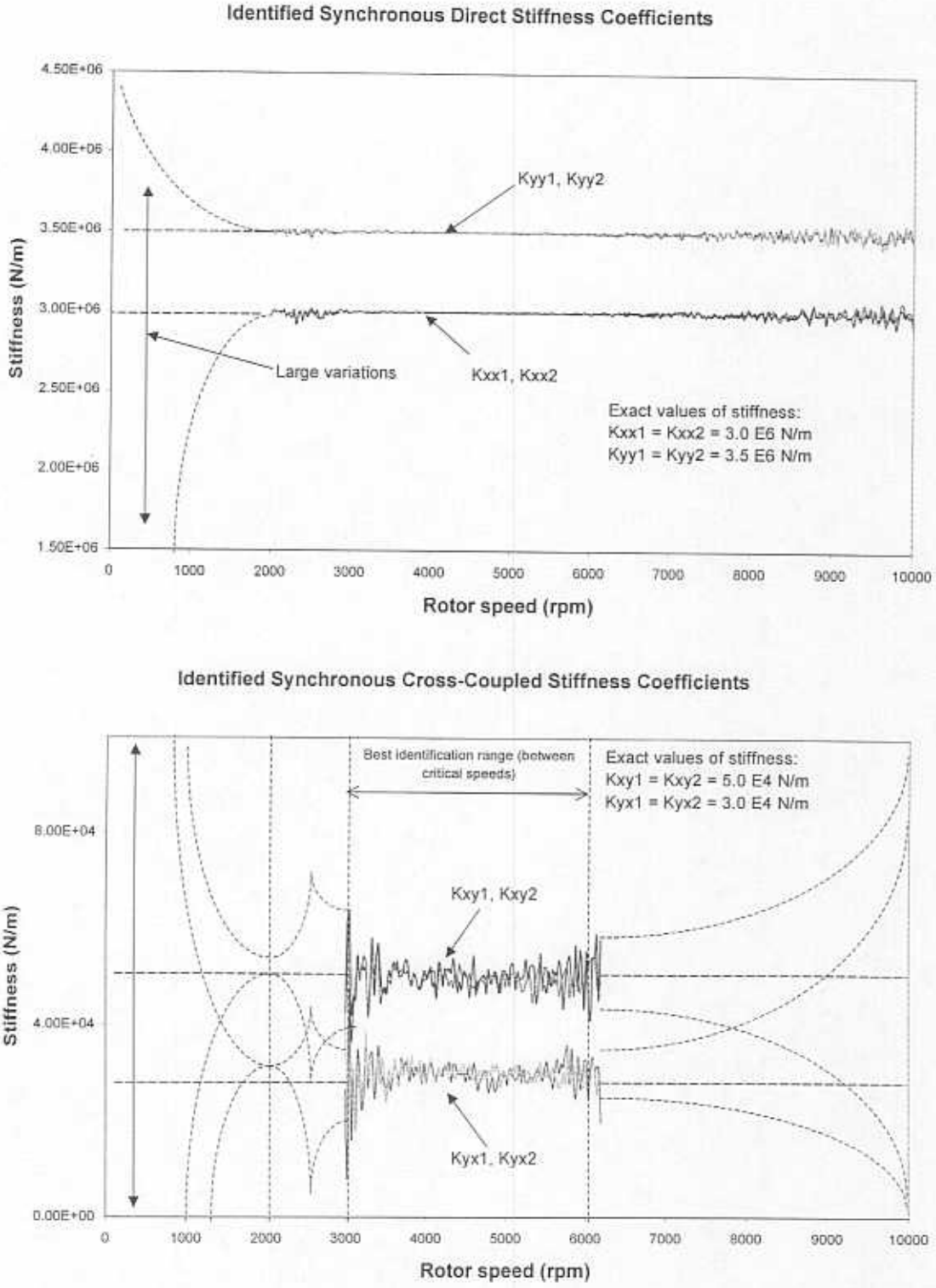

Figure 4a. Identified synchronous rotordynamic force coefficients from imbalance response. Parameters from numerical experiment.

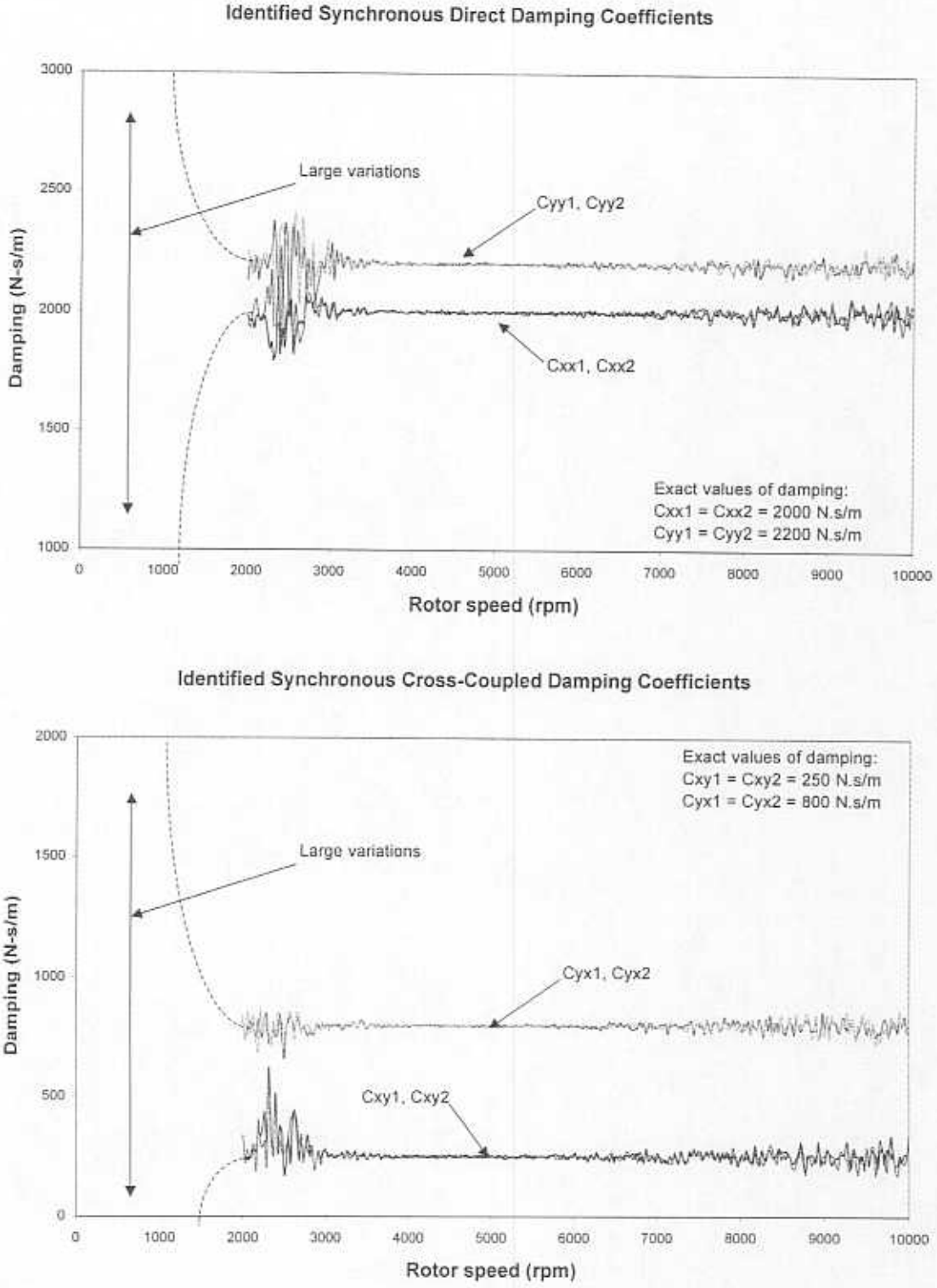

Figure 4b. Identified synchronous rotordynamic force coefficients from imbalance response. Parameters from numerical experiment.

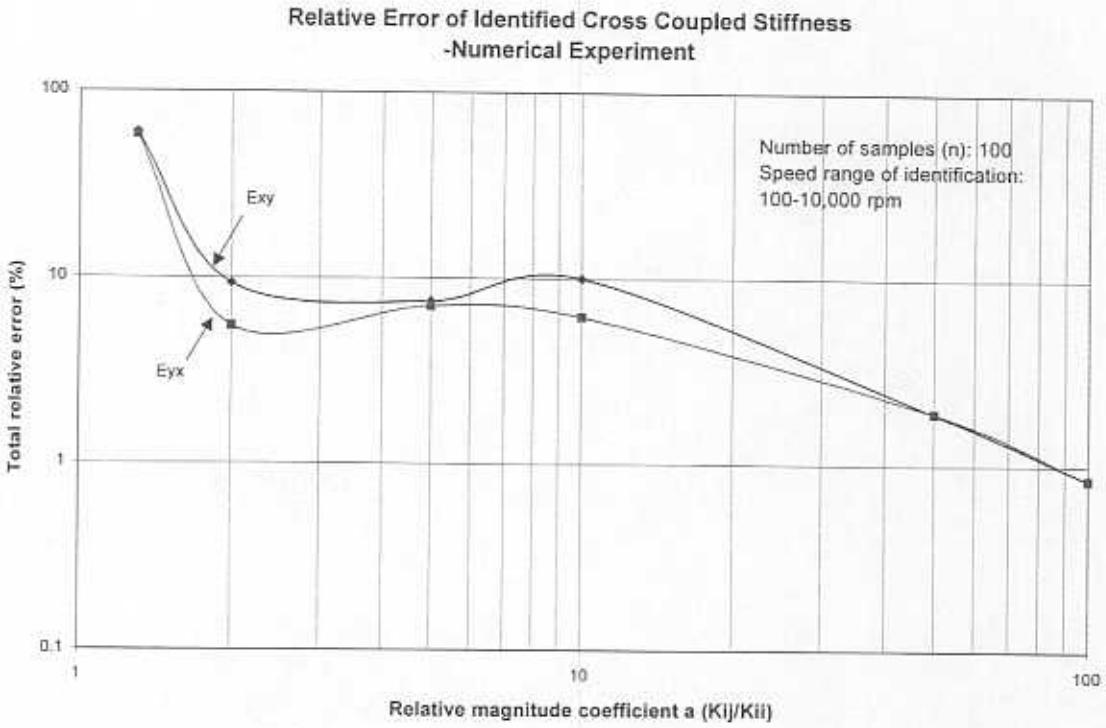

Figure 5. Sensitivity of identification method to cross-coupled to main stiffness ratio for identification of cross-coupled coefficients.

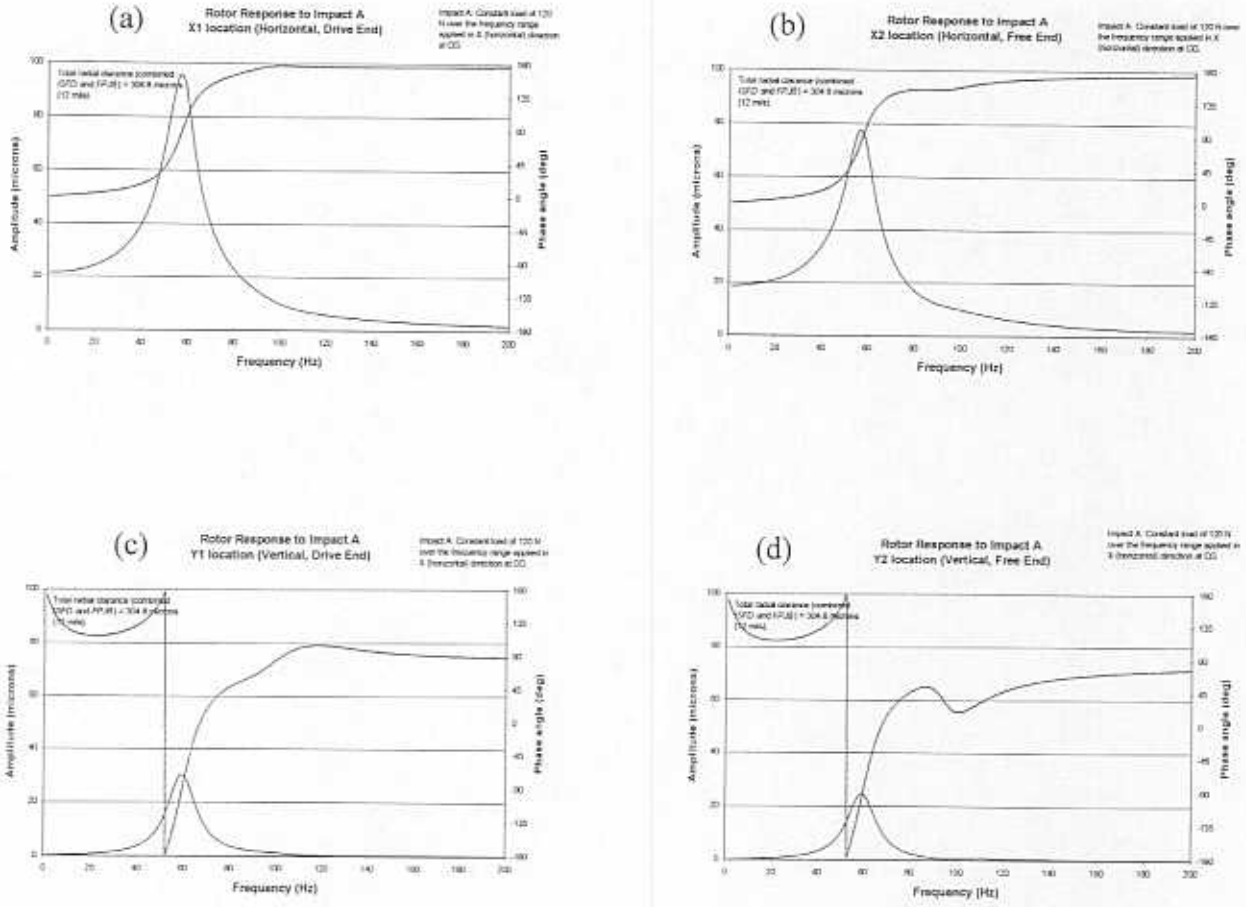

Figure 6a. Theoretical frequency response of rigid rotor to ideal impacts at rotor CG in horizontal direction (Test A). Rotor speed: 1000 rpm. (a) Drive end, horizontal, (b) Free end, horizontal, (c) Drive end, vertical, (d) Free end, vertical.

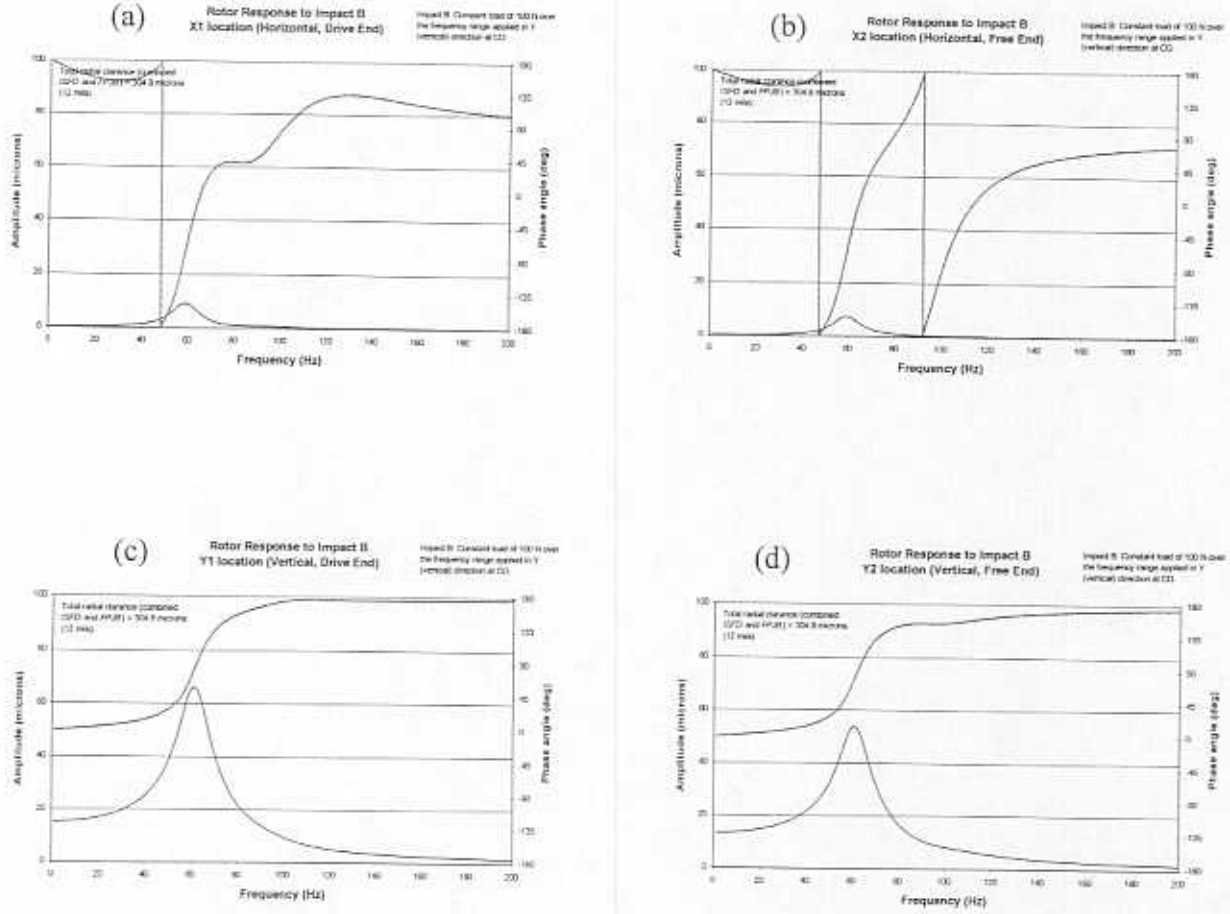

Figure 6b. Theoretical frequency response of rigid rotor to ideal impacts at rotor CG in vertical direction (Test B). Rotor speed: 1000 rpm. (a) Drive end, horizontal, (b) Free end, horizontal, (c) Drive end, vertical, (d) Free end, vertical.

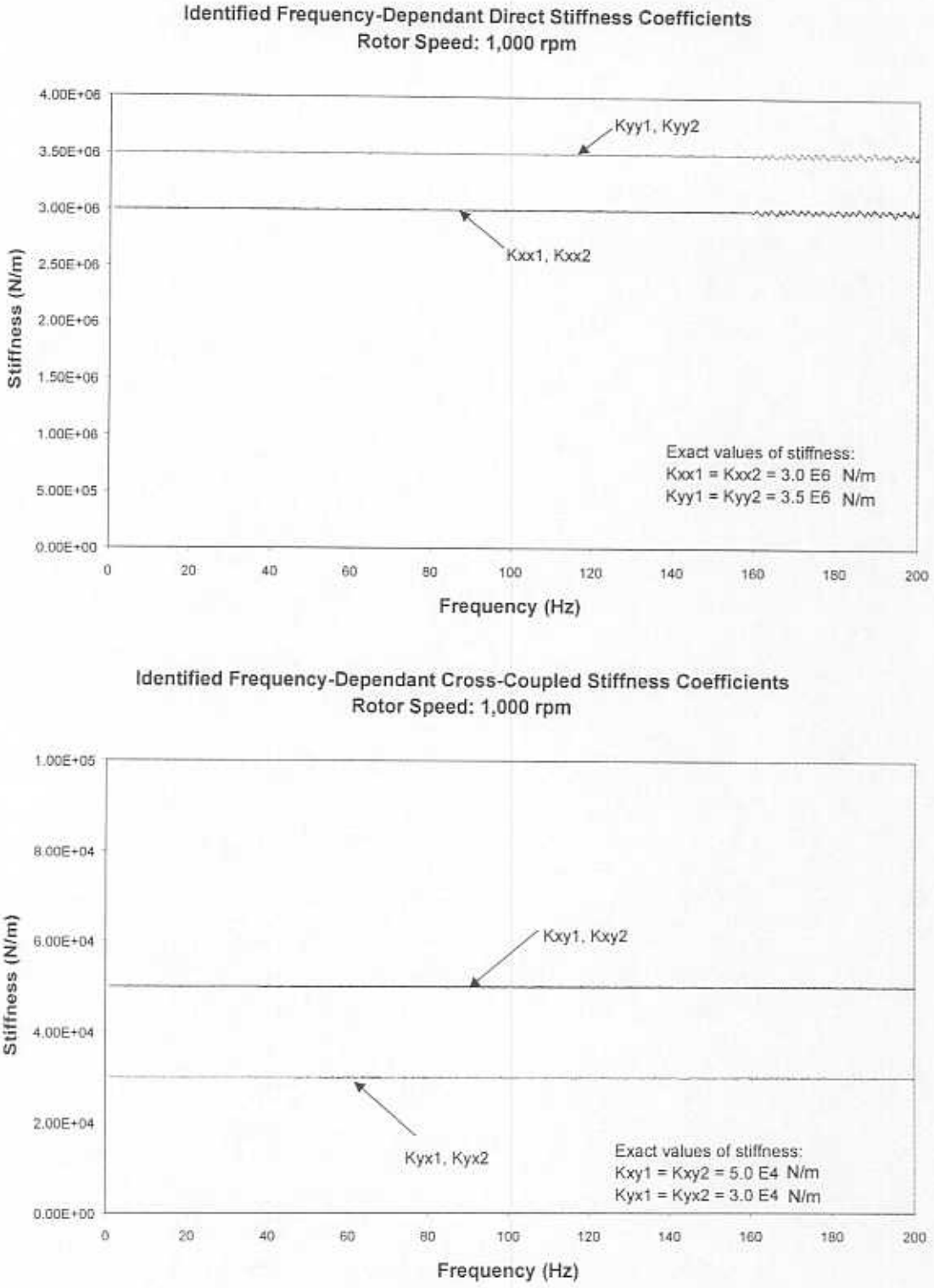

Figure 7a. Identified frequency-dependant rotordynamic force coefficients from impact response. Numerical experiment, rotor speed = 1,000 rpm.

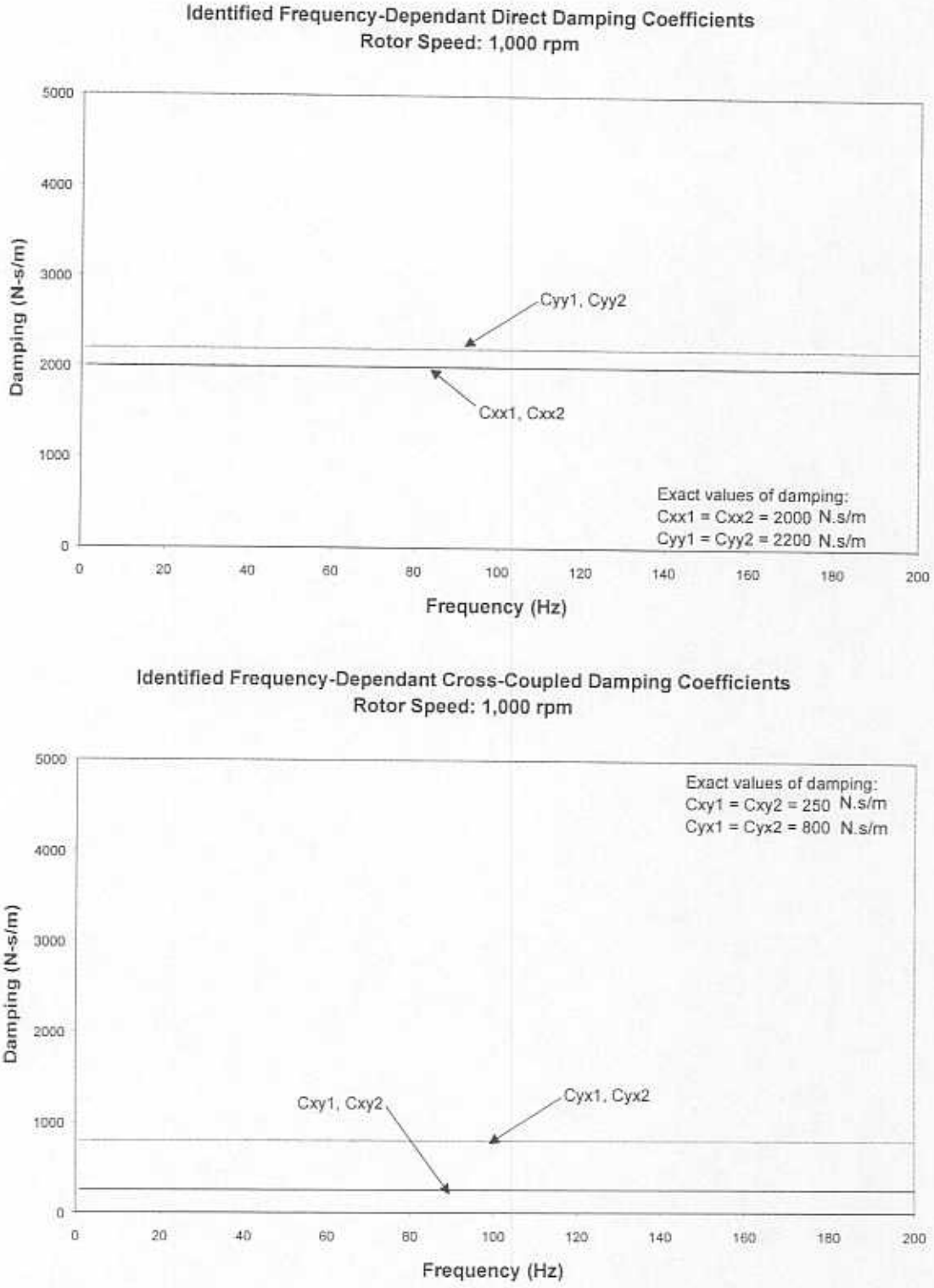

Figure 7b. Identified frequency-dependant rotordynamic force coefficients from impact response. Numerical experiment, rotor speed = 1,000 rpm.

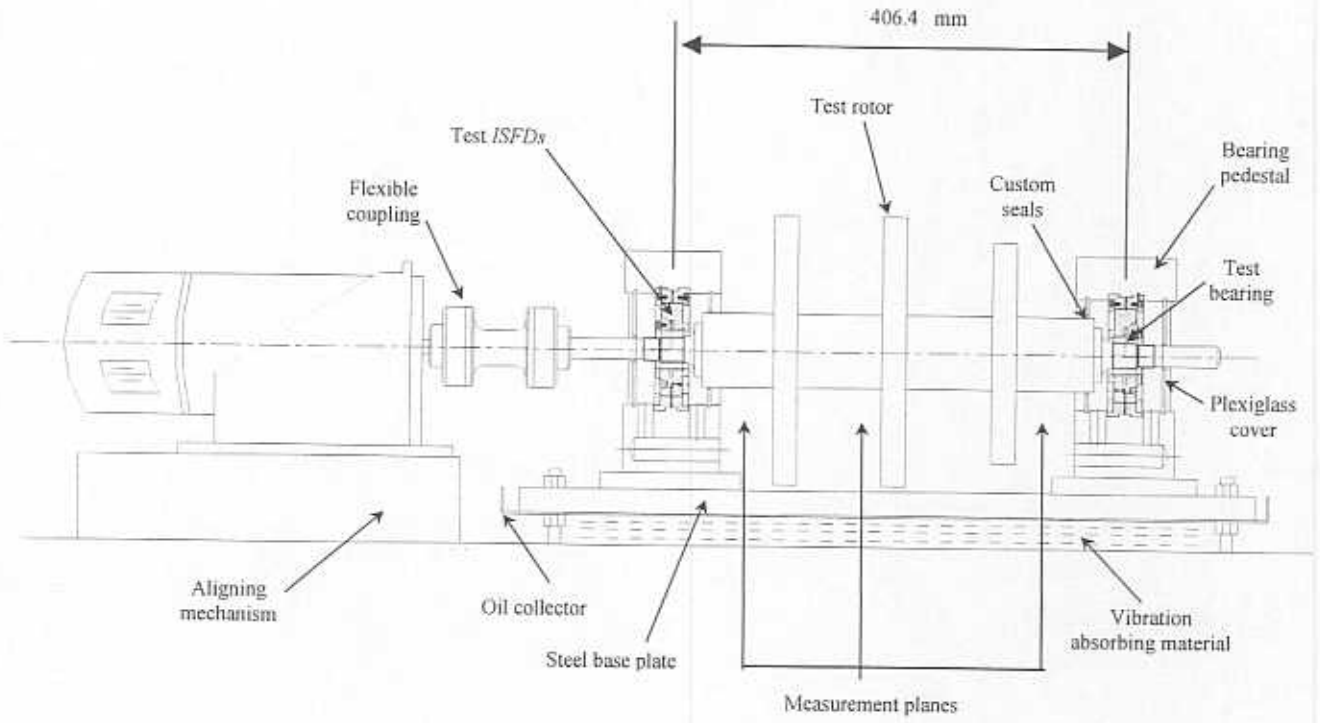

Figure 8. Test rig for measurements of imbalance response of rotor supported on tilting pad bearings and squeeze film dampers.

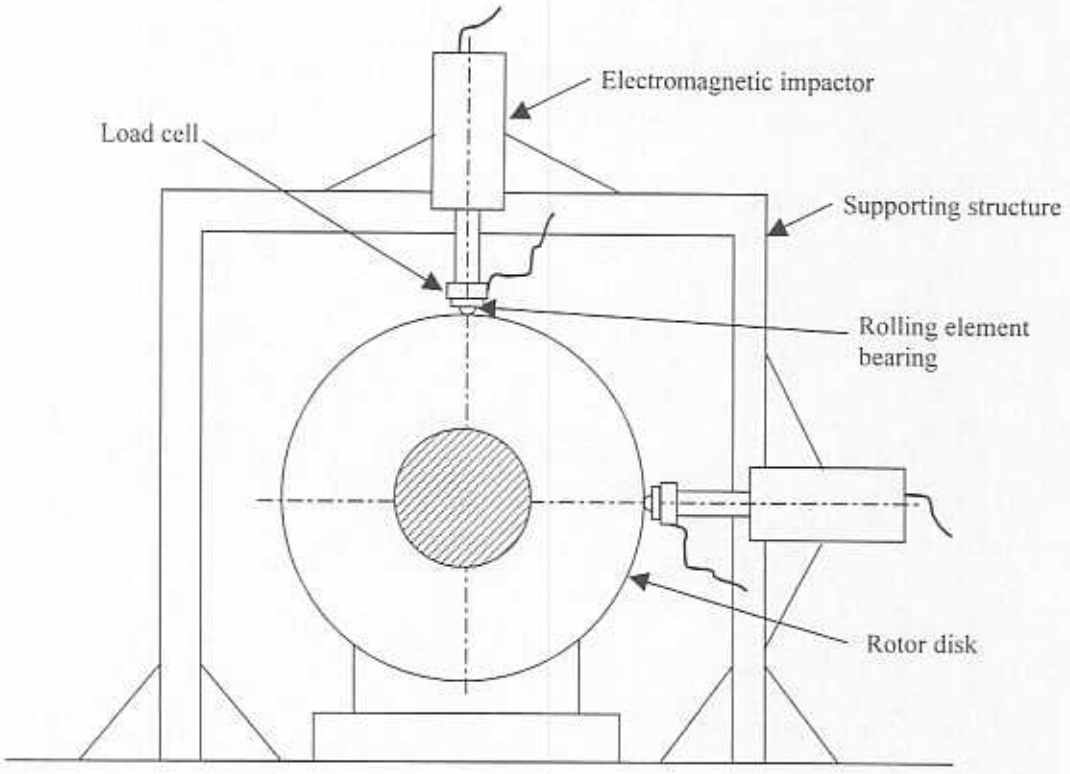

Figure 9. Cut-away view of test rotor showing electromagnetic impactor mechanisms in two orthogonal directions.

Appendix A
TEST RIG AND LUBRICATION SYSTEM DESCRIPTION

The test rig for measurements of imbalance response is the same rig used by De Santiago and San Andrés [10] in previous measurements of imbalance response, and is shown in Figure 8 in text. Two identical supports with series *FPJBs* and integral *SFDs* support the rotor as shown in Figure 8. The rig rests on a base plate bolted to a heavy worktable resting on an elastomeric vibration-absorbing pad. A 7.5 kW (10 HP) DC power supply and DC motor drive the test rotor through a flexible coupling. A *drawn cup* roller clutch in the coupling allows the motor to bring the rotor to a top speed of 10,000 rpm and then be shut off without applying a torque to the freely rotating shaft. This feature of the coupling ensures free coast down tests of the rig as the motor friction drag barely affects the rotor deceleration rate.

The rotor consists of a shaft, (673 mm, 26.5 in, long with main diameter 76.2 mm, 3 in) and three disks (25.4 mm, 1 in, thick) shrunk fitted at evenly spaced intervals of 63.5 mm (2.5 in). The two disks closer to the motor end are 279.4 mm (11 in) in diameter, and the third disk has a diameter of 228.6 mm (9 in). Each disk has twelve evenly spaced threaded holes at a radius of 114.3 mm (4.5 in) for the large disks and 95.25 mm (3.75 in) for the small disk. The threaded holes accommodate calibrated imbalance masses for harmonic response tests. The rotor assembly weighs 41.7 kg (92 lb) and is supported on a pair of flexure pivot tilting pad fluid film bearings, which are themselves mounted inside each damper journal as shown in Figure 2.

The bearing span of the test rig is 406 mm (16 in) with the rotor middle disk located halfway between the two supports. The bearing support housings are split elements with a 36 mm (1.42 in) wide groove at mid-length of their inner bore. This groove is the seat for the damper housings and it becomes a circumferential chamber that allows lubricant feeding to the damper film lands after the installation of each damper bearing. The lubricant feed port is located on the side (horizontal plane) of each bearing housing support, and drain ducts at the bottom collect the oil discharge from the fluid film bearings and squeeze film dampers. An independent circuit feeds the tilting pad bearings from the outer side faces of the integral dampers. An internal conduct machined in the damper journal serves as a plenum around the tilting pad bearing and small orifices located between the bearing pads serve as feeding ports to the fluid film bearing lands.

Figure A1 depicts the lubrication system delivering oil to the bearing housings (dampers) and fluid film bearings from a 151-lt (40-gal) reservoir through a variable speed gear pump. Turbine flow meters monitor the flow rate supplied to the fluid film bearings and dampers, and pressure gauges indicate the static supply pressure to each support element.

Three pairs of non-contact eddy-current displacement sensors measure the rotor displacement directly at locations next to the bearing (inboard side) on the motor drive end, the middle disk, and the bearing at the rotor free end. The displacement sensors are

mounted in the horizontal and vertical directions, at every plane. Several piezoelectric accelerometers are magnetically attached to the bearing support housings. An optical keyphasor facing the drive motor coupling provides a pick-up signal for measuring the rotor speed. Type-K thermocouples provide signals for measurement of the inlet oil, drive motor, and room temperatures.

A commercial data acquisition system installed on a personal computer record the rotor speed and the vibration signals from the six displacement sensors and two accelerometers. The data processing software includes real time slow-roll subtraction, synchronous response filtering and baseline response compensation. An instrumentation console contains digital displays of the operating rotor speed, flow rates, and measured temperatures. The console includes the controls for operation of the lubrication pumps and the oil cooling and heating elements. Three oscilloscopes display the rotor orbits at the monitored locations and a frequency analyzer depicts the FFT of selected vibration signals.

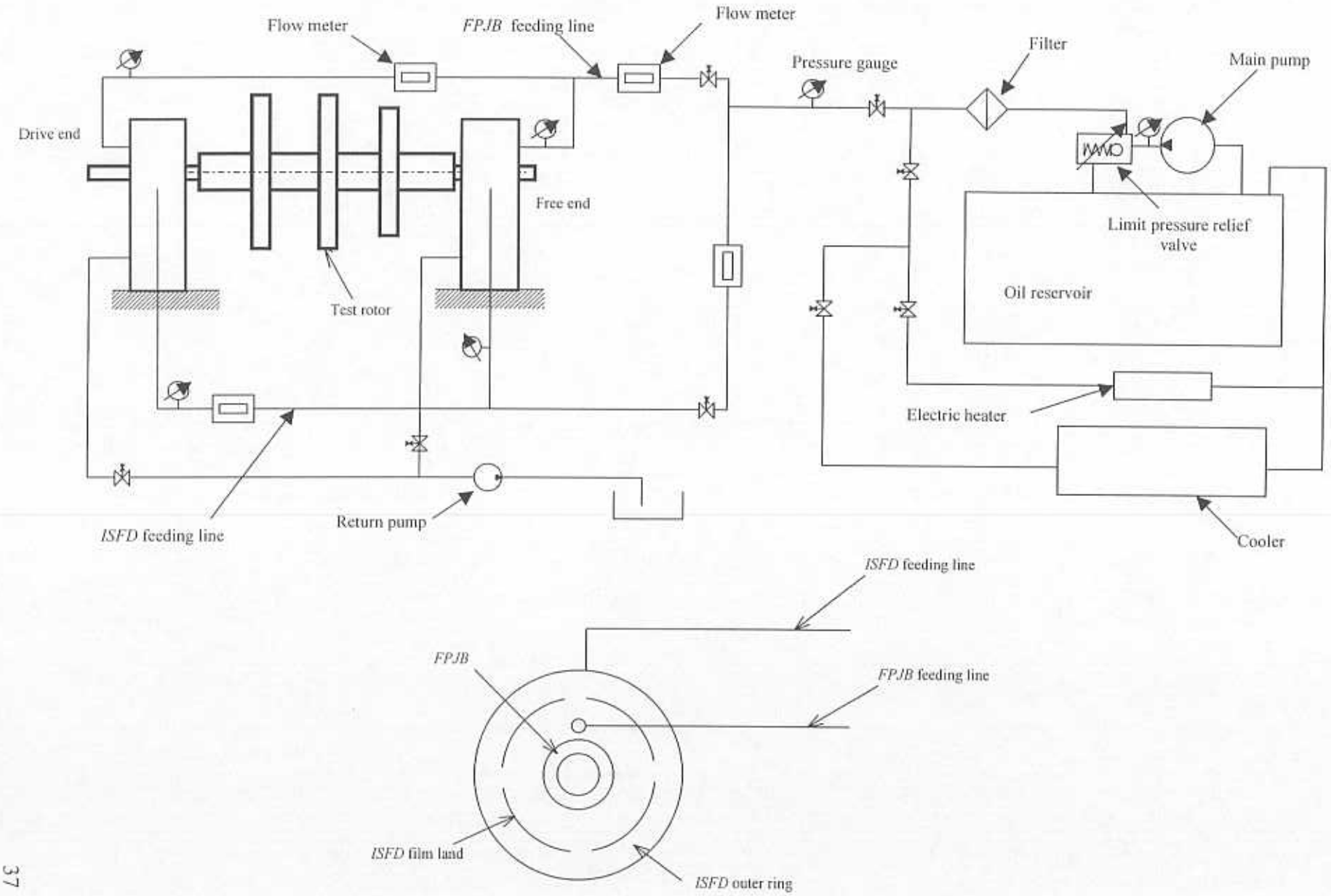

Figure A1. Lubrication system of squeeze film damper test rig.